



Potential applications of BFPF1 in Bcl-2 protein quantification, carcinoma cell visualization, cell sorting and early cancer diagnosis



Tao Liang, Jia Li, Yi Zhou, Xuben Hou, Xinying Yang^{**}, Hao Fang^{*}

Key Laboratory of Chemical Biology (Ministry of Education), School of Pharmaceutical Sciences, CheeLoo College of Medicine, Shandong University, 44, West Culture Road, 250012, Jinan, Shandong, PR China

ARTICLE INFO

Article history:

Received 29 December 2020
Received in revised form
3 July 2021
Accepted 26 July 2021

Keywords:

Bcl-2 protein fluorescence probe
Bcl-2 protein quantification
Carcinoma cell visualization
Cell sorting
Early cancer diagnosis

ABSTRACT

Overexpression of the Bcl-2 protein has emerged as a hallmark of carcinoma cells and can be employed as a biochemical biomarker of these cells. Therefore, some Bcl-2 protein fluorescence probes (**BFPFs**) were designed for Bcl-2 protein quantification and carcinoma cells labeling. The high Bcl-2 protein binding affinity ($K_i < 1$ nM) and selectivity (over 50,000-fold Bcl-2 protein selectivity against Mcl-1 protein) of **BFPF1** endow it with the ability to detect trace amounts of Bcl-2 protein. After being incubated with a range of concentrations of Bcl-2 protein, **BFPF1** exhibited the desired fluorescence properties and its fluorescence intensity is proportional to Bcl-2 protein concentration. Therefore, **BFPF1** provides a convenient approach for Bcl-2 protein quantification and we could determine the concentration of Bcl-2 protein based on the **BFPF1**'s fluorescence intensity. Subsequent studies revealed that **BFPF1** can fluorescently label carcinoma cells by binding to overexpressed Bcl-2 protein in living cells, and can distinguish carcinoma cells (HL-60 cells and ACHN cells) from normal-tissue cells (HUVECs) according to the different Bcl-2 protein expression levels between carcinoma cells and normal tissue cells. In the present study, **BFPF1** represents a new tool for Bcl-2 protein quantification, carcinoma cell visualization and cell sorting. Moreover, **BFPF1** can be used in the future for early cancer diagnosis by detecting carcinoma cells in patient tissues.

© 2021 Elsevier Masson SAS. All rights reserved.

1. Introduction

The growing incidence of cancer, a major health problem, has attracted people's attention around the world [1–6]. Decades of efforts have led to the development of various significant therapeutic regimens for cancer, whereas the overall five-year survival rate of patients remains low because of the delay in cancer diagnosis and the difficulty of cancer treatment [1,7–9]. Accumulating evidence revealed that early cancer diagnosis is central to the achievement of better outcomes and that effective clinical management of cancer is enabled by early cancer detection [10–13]. Although some methods have been developed for early cancer diagnosis [14–19], the lack of effective tools and bureaucratic procedures have greatly hindered the development of early cancer diagnosis [20]. In the present study, we sought to develop an effective and convenient tool for early cancer diagnosis.

Bcl-2 family proteins are the cardinal regulators of the mitochondrial pathway and they are subdivided into three groups according to the functions and Bcl-2 homology (BH) domains: anti-apoptotic proteins (Bcl-2, Mcl-1, Bcl-X_L, and Bcl-w, etc.), pro-apoptotic proteins (Bax, Bak, and Bok) and BH3-only proteins (Bax, Bid, Bim, Noxa, and Puma, etc.) [21,22]. The complex interactions between Bcl-2 family proteins regulate the apoptosis process, whereas overexpression of anti-apoptotic proteins prevents the activation of pro-apoptotic proteins, thereby abolishing the apoptosis event [23–26]. Accumulating evidence indicates that carcinoma cells frequently overexpress anti-apoptotic proteins, especially anti-apoptotic protein Bcl-2, to escape apoptosis [27–29]. Overexpression of Bcl-2 protein has emerged as a hallmark of carcinoma cells [30–34] and can be employed as a biochemical biomarker to identify carcinoma cells. Moreover, carcinoma cells can be distinguished from normal-tissue cells

* Corresponding author.

** Corresponding author.

E-mail addresses: xinyingyang@sdu.edu.cn (X. Yang), haofangcn@sdu.edu.cn (H. Fang).

according to the expression level of Bcl-2 protein with normal-tissue cells expressing less Bcl-2 protein than carcinoma cells. Therefore, the tool for Bcl-2 protein quantification in living cells can be also applied in carcinoma cell visualization, cell sorting and early cancer diagnosis.

Fluorescence probes can be powerful tools and are widely used in diverse fields [35–38]. Some Bcl-2 protein fluorescence probes have been developed but their poor Bcl-2 protein affinities and Bcl-2 protein selectivity make it difficult to achieve Bcl-2 protein quantification [39]. Therefore, we need a Bcl-2 protein fluorescence probe with very high Bcl-2 protein binding affinity, Bcl-2 protein selectivity as well as the desired fluorescence properties to achieve Bcl-2 protein quantification. Decades of efforts have developed some compounds targeting Bcl-2 protein [40–43] and ABT-199 (Venetoclax) was identified as the molecule with the highest Bcl-2 protein binding affinity ($K_i < 1$ nM) and selectivity [44]. To achieve above aims and improve the rationality of the Bcl-2 protein fluorescence probe, we sought to modify the structure of ABT-199, and develop an ABT-199-based Bcl-2 protein fluorescence probe. Before that, the binding mode of ABT-199 to Bcl-2 protein (PDB ID: 2O2F) was studied, and the results suggested that the tetrahydro-1,1'-biphenyl fragment accommodates the P2 pocket and the 1H-pyrrolo[[2,3-b]]pyridine fragment occupies the P4 pocket, whereas the 4-chloro-3-nitrobenzenesulfonamide group is exposed to the solvent (Fig. 1A). Given the importance of these functional fragments, we set out to retain these fragments and replace the solvent-exposed fragment with a fluorescence group (Fig. 1B) to develop Bcl-2 protein fluorescence probes (BPFPs).

2. Results and discussion

2.1. Synthesis and characterization of BPFPs

The synthetic routes for target compounds are depicted in Scheme 1. As shown in Scheme 1, methyl 4-bromo-2-fluorobenzoate was reacted with 1-boc-piperazine to give intermediate **2**. The nucleophilic aromatic substitution reaction between intermediate **2** and 5-hydroxy-7-azaindole was performed to synthesize compound **3**. After removing the t-butyloxy carbonyl group, Borch reduction was conducted to prepare key intermediate **5** using compounds **4** and 4'-chloro-5,5-dimethyl-3,4,5,6-tetrahydro-[1,1'-biphenyl]-2-carbaldehyde. The hydrolysis reaction was simply used

to obtain intermediate **6**, which was converted into **BPFPs1-4** by coupling with different fluorescence group. The structures of intermediates and **BPFPs1-4** were characterized by ^1H NMR, ^{13}C NMR, and High-Resolution Mass Spectrometry (HRMS).

2.2. Bcl-2 protein binding affinities and selectivities

The Bcl-2 protein binding affinities and selectivities of **BPFPs1-4** were evaluated using the competitive fluorescence polarization binding assay with ABT-199 as the positive control. As shown in Table 1, the Bcl-2 protein binding affinities of **BPFP1** ($K_i < 1$ nM) and **BPFP2** ($K_i < 1$ nM) were comparable to the affinity of the positive control, ABT-199 ($K_i < 1$ nM). However, **BPFP3** and **BPFP4** showed low Bcl-2 protein binding affinities due to the lack of the acyl-sulfonamide group. None of the tested compounds showed significant Mcl-1 protein binding affinity ($K_i > 50000$ nM). It's to be noted that **BPFP1** and **BPFP2** exhibit very high Bcl-2 protein affinities and over 50000-fold Bcl-2 protein selectivity against Mcl-1 protein. Their high Bcl-2 protein binding affinities and selectivities endowed them with the ability to specifically detect trace amounts of Bcl-2 protein.

2.3. Proposed binding mode of BPFP1 and BPFP2 within Bcl-2 protein

BPFP1 and **BPFP2** were docked into the Bcl-2 protein binding site (PDB ID: 2O2F) by means of GLIDE (version 11.5, Schrodinger). As shown in Fig. 2A, **BPFP1** accommodates the P2 pocket as well as P4 pocket well, and the binding mode of **BPFP1** (docking score, -7.042) is similar to that of ABT-199 (docking score, -7.179). Moreover, a strong interaction was observed between the acyl-sulfonamide group of **BPFP1** and the W141 residues of Bcl-2 protein (Fig. 2B). In addition, **BPFP2** (docking score, -4.398) can be tolerated by P2 pocket and P4 pocket (Fig. 2D), whereas no hydrogen bond interaction was monitored (Fig. 2D).

2.4. Spectroscopic properties of BPFPs

As summarized in Table 2, **BPFP1** possesses an excitation wavelength at 340 nm, an emission wavelength at 520 nm and a good fluorescence quantum yield (28.3%). Moreover, **BPFP2** exhibits similar spectroscopic properties but its fluorescence

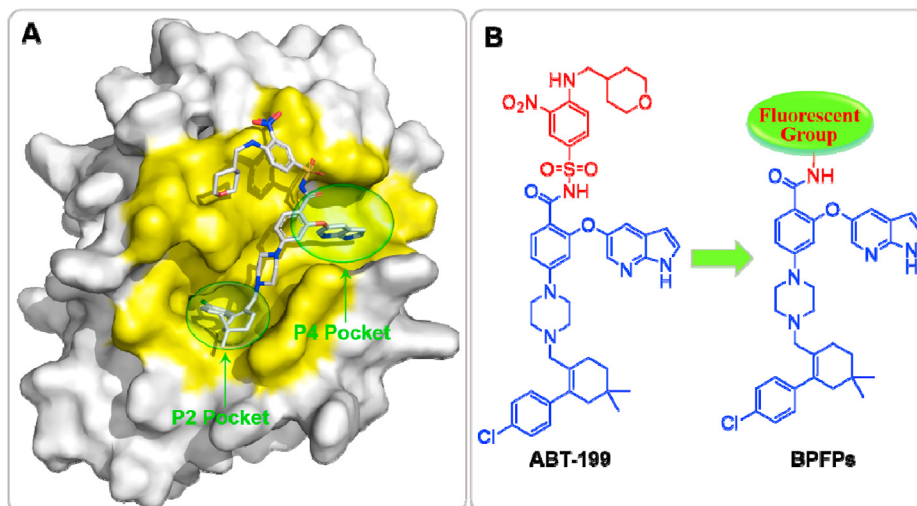
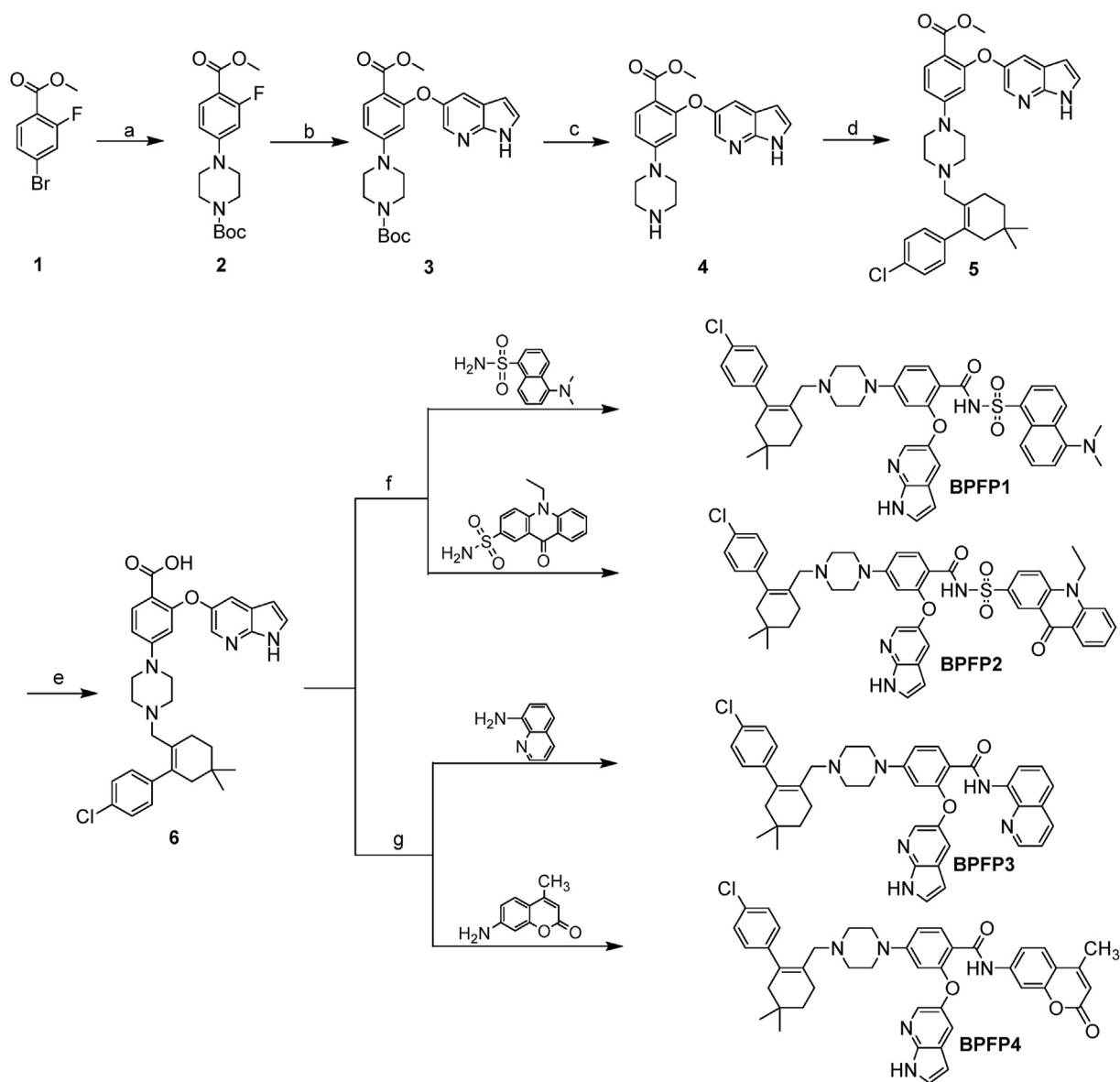


Fig. 1. (A) Binding mode of ABT-199 to Bcl-2 protein; (B) Design of the BPFPs.



Scheme 1. Synthetic Route of BPFPs 1-4^a.

^aRegents and Condition: (a) *N*-Boc-piperazine, Pd(AcO)₂, toluene, 60 °C, 6h, 81%; (b) 1H-pyrrolo[2,3-b]pyridin-5-ol, NaH, DMF, 120 °C, 8h, 76%; (c) (i) HCl/ethyl acetate, ethyl acetate, (ii) Saturated NaHCO₃, ethyl acetate, 1h, 96%; (d) 4'-chloro-5,5-dimethyl-3,4,5,6-tetrahydro-[1,1'-biphenyl]-2-carbaldehyde, NaBH(AcO)₃, rt, overnight, 79%; (e) KOH, THF/MeOH/H₂O = 1:3:1, refluxed, 6h, 89%; (f) Isobutyl chloroformate, 4-methylmorpholine, NaH, DMF, 80 °C, 8h, 60–62%; (g) HATU, DIEA, DMF, 60 °C, overnight, 47–61%.

quantum yield is low (0.7%). Therefore, the relatively reasonable fluorescence quantum yield of **BPFP1** suggested that **BPFP1** can be selected for further studies.

Table 1
Bcl-2 protein affinities and selectivities of BPFPs.

Compound	Bcl-2	Bcl-2 selectivity against Mcl-1
BPFP1	^a <i>K</i> _i < 1 nM	>50000-fold
BPFP2	<i>K</i> _i < 1 nM	>50000-fold
BPFP3	^b NA	–
BPFP4	NA	–
ABT-199	<i>K</i> _i < 1 nM	>50000-fold

^a All compounds were assayed three times.

^b NA, no activity.

2.5. Excitation and emission spectra of BPFP1 in different solvents

Subsequently, we explored the fluorescence excitation and emission spectra of **BPFP1** (1 μM) in different solvents. As we expected, the excitation spectra, emission spectra, and fluorescence intensity of **BPFP1** varied among the different solvents (Fig. 3). The experimental results suggested that the fluorescent properties of **BPFP1** change with the change of its environment. We think that **BPFP1** in a free state and **BPFP1** binding to Bcl-2 protein are in different environments. **BPFP1** in a free state not only has intramolecular motion, but also interacts with solvent molecules, which leads to a small amount of energy of the excited **BPFP1** molecule released in the form of fluorescence. However, **BPFP1** binding to Bcl-2 protein abolishes its intramolecular motion as well as intermolecular interaction and more energy of the excited **BPFP1** molecule is released in the form of fluorescence. Therefore, we

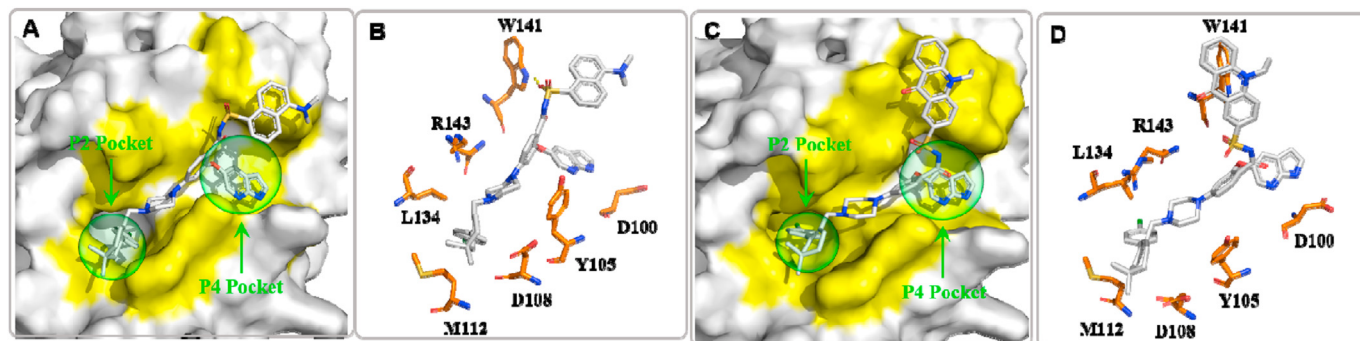


Fig. 2. (A) Proposed binding mode of BPF1 within the Bcl-2 binding site; (B) Interactions between BPF1 and Bcl-2 (PDB ID: 2O2F); (C) Proposed binding mode of BPF2 in the Bcl-2 binding site; (D) Interactions between BPF2 and Bcl-2 (PDB ID: 2O2F).

Table 2
Spectroscopic properties of the tested BPFs.

	λ_{\max} (nm)	λ_{exc} (nm)	λ_{em} (nm)	Φ (%)
BPF1	310	340	520	28.3
BPF2	332	350	480	0.7

speculated that incubating BPF1 with Bcl-2 protein might enhance its fluorescence.

2.6. Bcl-2 protein quantification and fluorescent properties of BPF1 Co-incubated with Bcl-2 protein or Mcl-1 protein

To confirm our hypothesis, we measured the fluorescence intensity of BPF1, which was incubated with a range of concentrations of Bcl-2 protein. As we expected, upon incubation with Bcl-2 protein, the fluorescence intensity of BPF1 was enhanced (Fig. 4A). Further studies revealed that BPF1's fluorescence intensity is proportional to Bcl-2 protein concentration (Fig. 4B). Therefore, BPF1 provides a convenient approach for Bcl-2 protein quantification and we could calculate the concentration of Bcl-2 protein based on the BPF1's fluorescence intensity.

As a potent and selective Bcl-2 inhibitor, ABT-199 exhibits strong Bcl-2 protein binding affinity ($K_i < 1$ nM) and it could compete with BPF1 for Bcl-2 binding sites. To determine whether the fluorescence enhancement was caused by the binding of BPF1 to Bcl-2 protein, 10 μM ABT-199 was co-incubated with 2 μM BPF1 and 0.125 mg/mL Bcl-2 protein. With the titration of ABT-199, BPF1 was competed from the Bcl-2 protein binding site. Then, we monitored a diminished fluorescence intensity, which is equivalent to BPF1's fluorescence intensity (Fig. 4C). The above results indicated that the binding of BPF1 to Bcl-2 protein enhances its fluorescence intensity.

To exclude the effect of Mcl-1 protein on the fluorescence intensity of BPF1, coincubation of BPF1 with 0.125 mg/mL Mcl-1 protein was performed. Following incubation with Mcl-1 protein, the fluorescence properties of BPF1 were determined but no change was observed (Fig. 4D). Thus, the presence of Mcl-1 protein does not affect the fluorescence properties of BPF1.

Combined with the above experimental results, we hypothesized the mechanism of the fluorescence enhancement of BPF1. We think that BPF1 in a free state possesses intramolecular motion which consumes the energy of excited BPF1, and little energy released as fluorescence. When BPF1 binding to Bcl-2 protein, restriction of intramolecular motion (RIM) of BPF1 occurs and more energy of excited BPF1 released as fluorescence, followed by the fluorescence enhancement of BPF1. As the protein concentration increases, more BPF1 binds to the Bcl-2 protein and more restriction of intramolecular motion (RIM) of BPF1 occurs, that results in the fluorescence of BPF1 being proportional to the Bcl-2 protein concentration.

2.7. Fluorescence imaging

Encouraged by the good properties of BPF1, fluorescence imaging of carcinoma cells (ACHN cells) and normal-tissue cells (HUVECs) was performed. Upon incubation with 1 μM BPF1, ACHN cells were fluorescently labeled, and strong green fluorescence was observed (Fig. 5A), whereas the addition of ABT-199 (5 μM) quenched the fluorescence (Fig. 5B). Moreover, after incubating BPF1 (1 μM) with HUVECs in the presence or absence of ABT-199 (5 μM), none of the HUVECs emitted fluorescence (Fig. 5C and D). The distinct results of fluorescence imaging on carcinoma cells (ACHN cells) and normal-tissue cells (HUVECs) indicated that BPF1 can selectively label carcinoma cells with green fluorescence and spare normal-tissue cells.

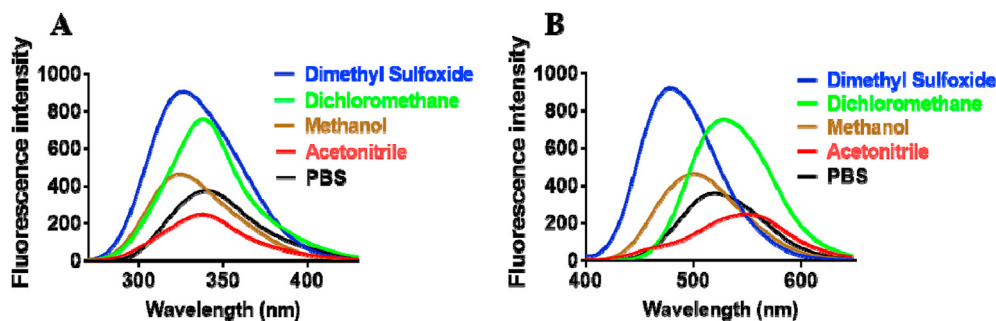


Fig. 3. Excitation spectra and emission spectra of BPF1 (1 μM) in different solvents.

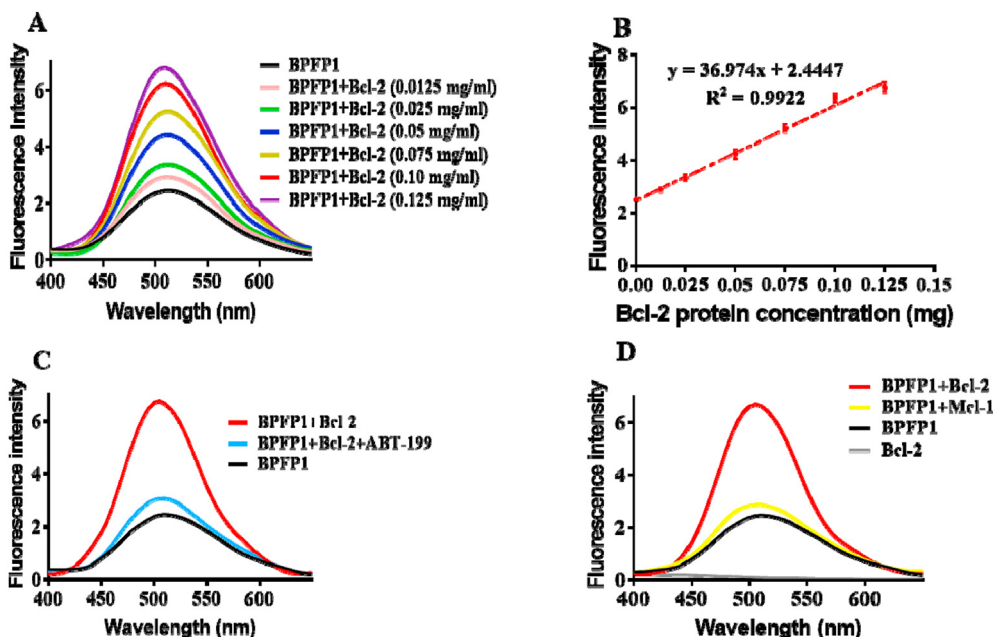


Fig. 4. (A) Fluorescence emission spectra of 2 μM BPFPP1 incubated with a range of concentrations of Bcl-2 protein; (B) Linear correlation between BPFPP1's fluorescence intensity and Bcl-2 protein concentration; (C) Fluorescence emission spectra of 2 μM BPFPP1, 2 μM BPFPP1+0.125 mg/mL Bcl-2 protein, and 2 μM BPFPP1+10 μM ABT-199 + 0.125 mg/mL Bcl-2 protein; (D) Fluorescence emission spectra of 2 μM BPFPP1, 0.125 mg/mL Bcl-2 protein, 2 μM BPFPP1+0.125 mg/mL Bcl-2 protein, and 2 μM BPFPP1+0.125 mg/mL Mcl-1 protein.

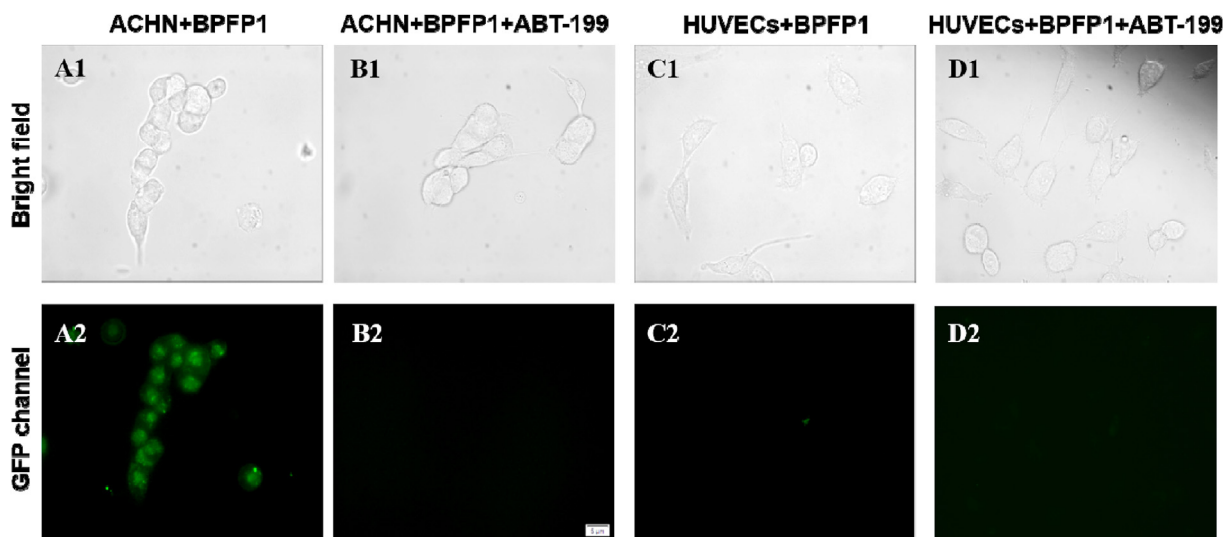


Fig. 5. Fluorescence imaging. (A) ACHN cells incubated with 1 μM BPFPP1; (B) ACHN cells incubated with 1 μM BPFPP1 and 5 μM ABT-199; (C) HUVECs incubated with 1 μM BPFPP1; (D) HUVECs incubate with 1 μM BPFPP1 and 5 μM ABT-199. Objective lens: 63 \times .

2.8. Colocalization analysis

To confirm whether BPFPP1 labels carcinoma cells by binding to Bcl-2 protein in living cells, colocalization analysis was performed. Commercial mitochondrial dye (MitoTracker Red CMXRos), nuclear dye (Hoechst 33342) and BPFPP1 were co-incubated with ACHN cells. As shown in Fig. 6, mitochondria were stained red by 300 nM MitoTracker Red CMXRos (Fig. 6A), whereas nuclei were stained blue by 10 $\mu\text{g}/\text{mL}$ Hoechst 33342 (Fig. 6C). After merging Fig. 6A, 6B, and 6C, we found that the area stained by the mitochondrial dye completely overlapped with the area stained by BPFPP1. These results indicated that BPFPP1 can label carcinoma cells by binding to protein located on mitochondria. Considering that our BPFPP1

specifically targets Bcl-2 protein and that Bcl-2 protein is generally located on mitochondria [45], we concluded that our BPFPP1 labels carcinoma cells by binding to Bcl-2 protein in living cells.

2.9. Flow-cytometry analysis

Before performing cell sorting, we analyzed the fluorescence properties of cells treated with BPFPP1. Carcinoma cells (ACHN cells and HL-60 cells) and normal-tissue cells (HUVECs) were chosen. As shown in Fig. 7, upon treatment with BPFPP1 (1 μM), ACHN cells and HL-60 cells were fluorescently labeled, but the additions of 5 μM ABT-199 quenched the fluorescence. HUVECs show no change after incubation with BPFPP1 because there is little Bcl-2 protein in

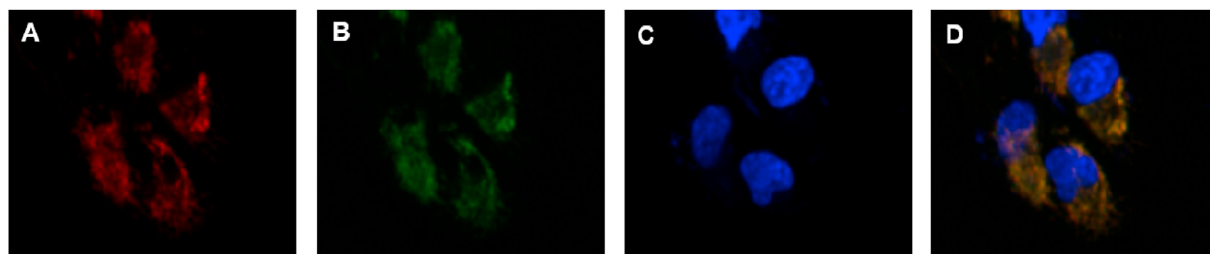


Fig. 6. (A) ACHN cells incubated with 300 nM MitoTracker Red CMXRos; (B) ACHN cell incubated with 1 μ M BPF1 (green channel); (C) ACHN cells incubated with 10 μ g/mL Hoechst 33342; (D) Merged image of panels of A, B and C.

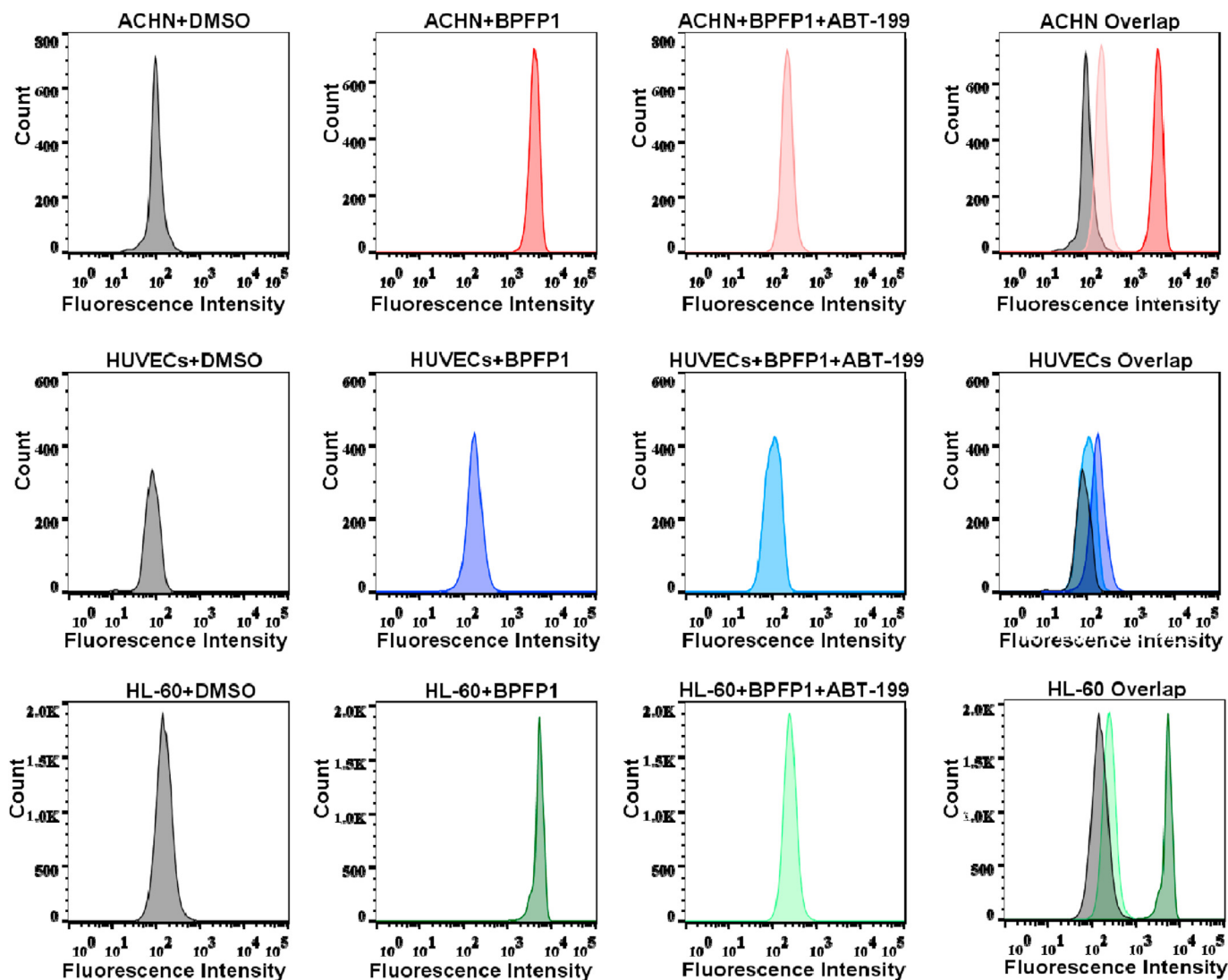


Fig. 7. Flow-cytometry analysis of ACHN cells, HL-60 cells, and HUVECs treated with 1 μ M BPF1 or DMSO for 20 min in the presence or absence of 5 μ M ABT-199.

HUVECs (Fig. S17). These results are consistent with the fluorescence imaging.

2.10. Cell sorting and cell line identification

The flow-cytometry analysis revealed that carcinoma cells and normal-tissue cells exhibit different fluorescence properties after being incubated with 1 μ M BPF1. Therefore, cell sorting was

designed based on the distinct fluorescence properties of carcinoma cells and normal-tissue cells. After incubating with 1 μ M BPF1 for 20 min, the solid tumor model (ACHN cells + HUVECs) and the hematoma model (HL-60 cells + HUVECs) were analyzed using a flow cytometer. As shown in Fig. 8A, cells in the solid tumor model were divided into two groups according to their distinct fluorescence properties. The cells in the hematoma model were also divided into two groups (Fig. 8B). Then, the fluorescently

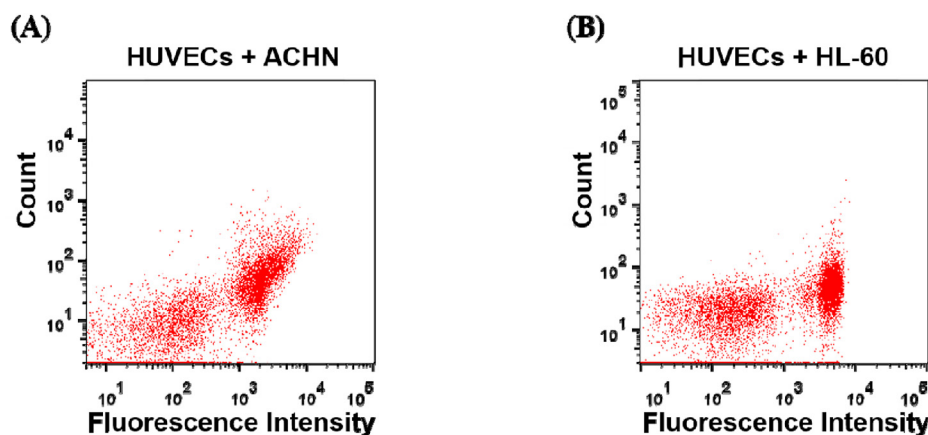


Fig. 8. Cell sorting of the solid tumor model (A) and the hematoma model (B).

labeled cells were sorted, and their short tandem repeat (STR) profiles were searched and compared in two recognized repositories (ATCC, DSMZ).

The STR profiles analysis suggested that the fluorescently labeled cells in the solid tumor model and the hematoma model were ACHN and HL-60 carcinoma cells, respectively (SI, Table S1 and Table S2). These results suggested that **BPFP1** could distinguish carcinoma cells and normal-tissue cells according to the cellular expression level of Bcl-2 protein. Given that **BPFP1** can detect, label and sort carcinoma cells from a mixture of carcinoma cells and normal-tissue cells, we think **BPFP1** can be used for early cancer diagnosis by detecting and sorting carcinoma cells in patient tissues.

2.11. The effect of **BPFP1** on cellular Bcl-2 protein expression

Western blot analysis was performed to explore whether **BPFP1** affects the expression of Bcl-2 protein in living cells. As shown in Fig. 9, treatment with **BPFP1** does not affect the expression of Bcl-2 protein in ACHN cells, HL-60 cells and HUVECs.

2.12. Cytotoxicity studies

We evaluated the cytotoxicity of **BPFP1** and ABT-199. Following cell treatment with a range of concentrations of **BPFP1** and ABT-199 for 1 hour, the viabilities of ACHN cells, HL-60 cells, and HUVECs were determined with a CCK-8 kit. As shown in Fig. 10, both **BPFP1** and ABT-199 exhibit acceptable cytotoxicity.

3. Conclusions

In summary, a series of Bcl-2 protein fluorescence probes (**BPFPs**) were designed rationally. Preliminary studies suggested that **BPFP1**, exhibits very strong Bcl-2 protein binding affinity ($K_i < 1$ nM) and over 50000-fold Bcl-2 protein selectivity. The high Bcl-2 protein binding affinity and selectivity endow **BPFP1** with the ability to detect Bcl-2 protein efficiently and specifically. After being incubated with a range of concentrations of Bcl-2 protein, **BPFP1** exhibited the desired fluorescence properties and its fluorescence intensity is proportional to Bcl-2 protein concentration. Therefore, **BPFP1** provides a convenient approach for Bcl-2 protein quantification and we could calculate the concentration of Bcl-2 protein according to **BPFP1**'s fluorescence intensity. Furthermore, fluorescence imaging assay and colocalization analysis confirmed that **BPFP1** can fluorescently label carcinoma cells by binding to cellular

overexpressed Bcl-2 protein. Subsequently, **BPFP1** was applied in cell sorting and found to successfully distinguished carcinoma cells from normal-tissue cells by detecting the different Bcl-2 protein expression levels between carcinoma cells and normal-tissue cells. As a powerful tool, **BPFP1** has been successfully applied in this study to Bcl-2 protein quantification, carcinoma cell visualization and cell sorting, and it can be used in the future for early cancer diagnosis by detecting carcinoma cells in patient tissues.

4. Experimental

4.1. Materials and instrumentation

Recombinant human Bcl-2 and Mcl-1 proteins were obtained from Shanghai Institute of Organic Chemistry, Chinese Academy of Sciences; Primary antibodies were purchased from Cell Signaling Technology (CST), ACHN cell, HL-60 cell, and HUVEC cell were purchased from American-type culture collection (ATCC). Other biological reagents were purchased from Sigma-Aldrich, Biovision, Beyotime and Biotechnology. All chemical reagents are analytical grade and used without further purification unless otherwise stated. Reactions were monitored by thin-layer chromatography (TLC) on 0.25 mm silica gel plates (60 GF-254). Melting points were determined by the RY-1 electrothermal melting point apparatus. ^1H NMR and ^{13}C NMR spectra were obtained on a Bruker DRX spectrometer at 400 MHz. High-resolution mass spectra (HRMS) were conducted on an Agilent 6510 quadrupole time-of-flight liquid chromatography/mass spectrometer (LC/MS) delivered with electrospray ionization (ESI). Absorption and fluorescence spectra were recorded on a Thermo Varioskan microplate reader. Fluorescence imaging was obtained by a Zeiss Axio Observer A1 fluorescence microscope and a Zeiss LSM780 confocal fluorescence microscope; Flow cytometry analysis and cell sorting were conducted on Beckman Coulter MoFloAstrios EQ Flow Cytometer.

4.2. General procedures of **BPFPs1-4**

4.2.1. Tert-butyl 4-(3-fluoro-4-(methoxycarbonyl)phenyl)piperazine-1-carboxylate (2)

The reaction mixture of intermediate 1 (4.7 g, 20 mmol), 1-boc-piperazine (5.2 g, 28 mmol), Pd(OAc)₂ (0.224 g, 1 mol), BINAP (1.25 g, 2 mol), and Cs₂CO₃ (7.17 g, 22 mol) in dry toluene (200 mL) was stirred at 80 °C for 8 h. After cooling, the palladium catalyst as well as Cs₂CO₃ were removed by filtration through Celite pad and the solvent was removed. The crude product was recrystallized

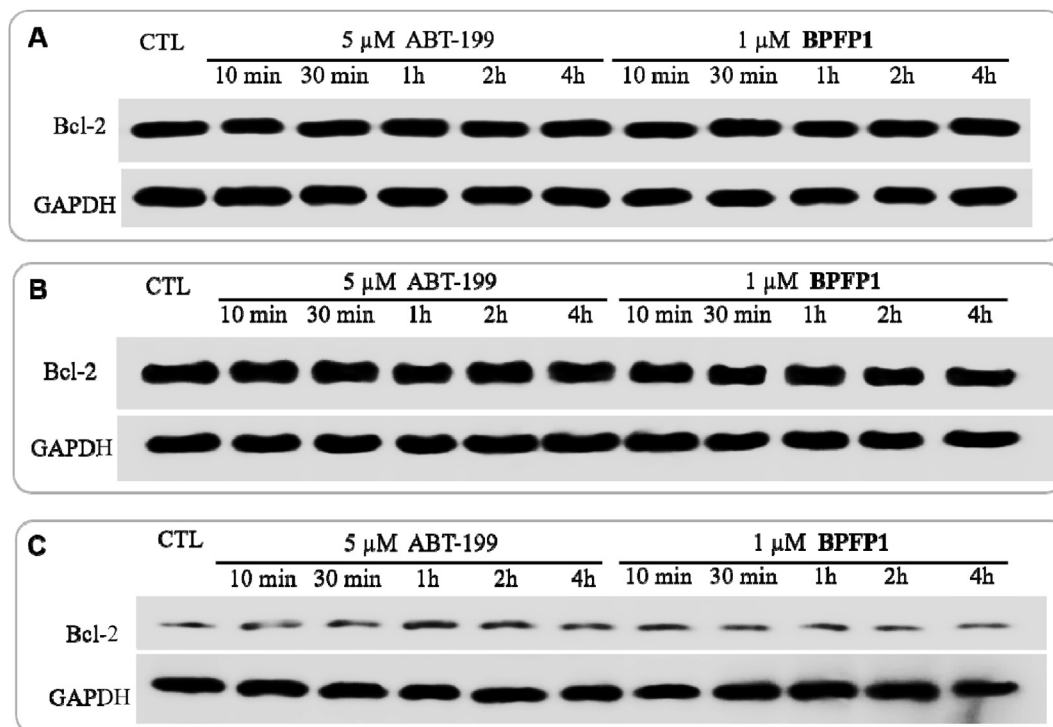


Fig. 9. Upon treatment with 1 μM BFPF1 or 5 μM ABT-199 for different durations, the Bcl-2 protein expression of ACHN cells (A), HL-60 cells (B), and HUVECs (C).

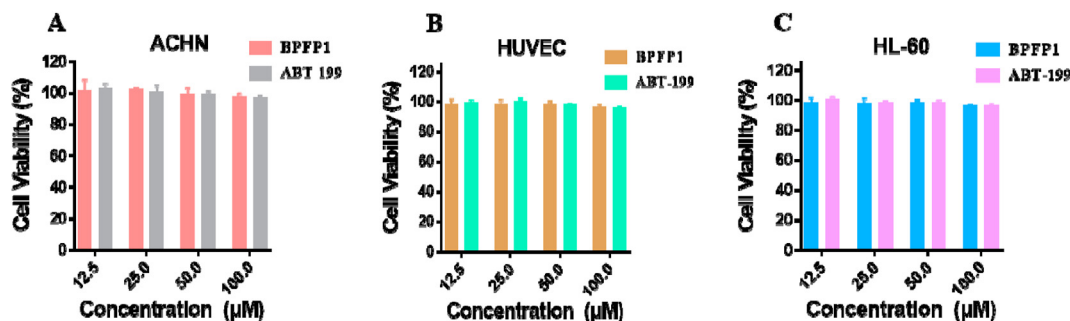


Fig. 10. Cell viabilities of ACHN cells (A), HUVECs (B), and HL-60 cells (C) treated with a range of concentrations of BFPF1 and ABT-199 (12.5, 25, 50 and 100 μM) for 1h.

with ethyl acetate to give white solid, 5.4 g. Yield: 81%, m.p 148–149 °C. ^1H NMR (400 MHz, CDCl_3) δ 7.84 (t, J = 8.8 Hz, 1H), 6.62 (dd, J = 8.9, 2.4 Hz, 1H), 6.51 (dd, J = 14.5, 2.3 Hz, 1H), 3.88 (s, 3H), 3.68–3.50 (m, 4H), 3.40–3.17 (m, 4H), 1.49 (s, 9H).

4.2.2. Tert-butyl 4-(3-((1H-pyrrolo[2,3-b]pyridin-5-yl)oxy)-4-(methoxycarbonyl)phenyl) piperazine-1-carboxylate (3)

To the solution of compound 2 (5.07 g, 15 mmol) in anhydrous *N,N*-dimethylformamide (120 mL), 1H-pyrrolo[2,3-b]pyridin-5-ol (2.1g, 15 mmol) as well as NaH (0.66g, 16.5 mmol) were added and the mixture was stirred at 120 °C for 8h. Cool the reaction mixture down and pour it into water (300 mL). Extract with ethyl acetate (150 ml \times 3) and dry the organic phase over with MgSO_4 for 0.5 h. The solvent was removed under vacuo to give the crude product, followed by purification by silica gel chromatography. White solid 5.16 g, yield: 76%. m.p 193–194 °C. ^1H NMR (400 MHz, $\text{DMSO}-d_6$) δ 11.64 (s, 1H), 8.01 (d, J = 2.5 Hz, 1H), 7.79 (d, J = 8.9 Hz, 1H), 7.48 (t, J = 2.8 Hz, 1H), 7.43 (d, J = 2.5 Hz, 1H), 6.79 (dd, J = 9.0, 2.1 Hz, 1H), 6.43 (d, J = 2.0 Hz, 1H), 6.38 (dd, J = 2.9, 1.8 Hz, 1H), 3.65 (s, 3H), 3.42 (t, J = 4.6 Hz, 4H), 3.21 (t, J = 4.7 Hz, 4H), 1.39 (s, 9H).

4.2.3. Methyl 2-((1H-pyrrolo[2,3-b]pyridin-5-yl)oxy)-4-(piperazin-1-yl)benzoate (4)

Dissolve compound 3 (4.5 g, 10 mmol) with ethyl acetate (60 mL) and HCl/EA (40 mL) was added. Stir the mixture overnight and the precipitation was filtered. To the mixture ethyl acetate (100 mL) and saturated NaHCO_3 (100 mL), the precipitation was added. Stir the mixture for 1h and extract with ethyl acetate. Dry the organic phase over with MgSO_4 and remove the solvent to give white solid, yield: 96%. m.p 146–148 °C. ^1H NMR (400 MHz, $\text{DMSO}-d_6$) δ 11.65 (s, 1H), 8.01 (d, J = 2.5 Hz, 1H), 7.77 (d, J = 9.0 Hz, 1H), 7.48 (t, J = 2.8 Hz, 1H), 7.44 (d, J = 2.5 Hz, 1H), 6.78 (dd, J = 9.0, 2.1 Hz, 1H), 6.46–6.29 (m, 2H), 3.66 (s, 3H), 3.16–3.05 (m, 4H), 2.81–2.62 (m, 4H).

4.2.4. Methyl 2-((1H-pyrrolo[2,3-b]pyridin-5-yl)oxy)-4-(4-(4'-chloro-5,5-dimethyl-3,4,5,6-tetrahydro-[1,1'-biphenyl]-2-yl)methyl)piperazin-1-yl)benzoate (5)

To the solution of compound 4 (3.17g, 9 mmol) in 1, 2-dichloroethane (80 mL), 4'-chloro-5,5-dimethyl-3,4,5,6-tetrahydro-[1,1'-biphenyl]-2-carbaldehyde (2.46 g, 9.9 mmol) was added and

the mixture was stirred for 1 h. Then sodium triacetoxyborohydride (5.72 g, 27 mmol) was added and stirred the mixture for another 6 h. Filter and the organic phase was washed with saturated NaHCO₃ as well as saturated NaCl. The crude product was purified by silica gel chromatography to give white solid 4.16 g, yield: 79%. m.p 92–94 °C. ¹H NMR (400 MHz, DMSO-*d*₆) δ 11.63 (s, 1H), 7.99 (d, *J* = 2.5 Hz, 1H), 7.75 (d, *J* = 9.0 Hz, 1H), 7.50–7.46 (m, 1H), 7.42 (d, *J* = 2.3 Hz, 1H), 7.35 (d, *J* = 8.3 Hz, 2H), 7.05 (d, *J* = 8.3 Hz, 2H), 6.78–6.70 (m, 1H), 6.40–6.31 (m, 2H), 3.65 (s, 3H), 3.12 (m, 4H), 2.73 (m, 2H), 2.19 (m, 6H), 1.97 (d, *J* = 12.7 Hz, 2H), 1.39 (t, *J* = 6.3 Hz, 2H), 0.94 (s, 6H).

4.2.5. 2-((1*H*-pyrrolo[2,3-*b*]pyridin-5-yl)oxy)-4-(4-((4'-chloro-5,5-dimethyl-3,4,5,6-tetrahydro-[1,1'-biphenyl]-2-yl)methyl)piperazin-1-yl)benzoic acid (6)

To the solution of compound 5 (4.09 g, 7 mmol) in THF/MeOH/H₂O = 1:3:1 (60 mL), KOH (1.57 g, 28 mmol) was added, and refluxed the mixture for 6 h. Remove the organic phase and acidified it to pH 2 with 6 M HCl. Filter and wash the precipitation with water. White solid 3.56g, yield: 89%. m.p 249–250 °C. ¹H NMR (400 MHz, DMSO-*d*₆) δ 11.57 (s, 1H), 7.96 (s, 1H), 7.60 (d, *J* = 8.5 Hz, 1H), 7.42 (s, 1H), 7.35 (m, 3H), 7.05 (d, *J* = 7.8 Hz, 2H), 6.64 (d, *J* = 8.6 Hz, 1H), 6.33 (s, 1H), 6.29 (s, 1H), 3.03 (s, 4H), 2.73 (s, 2H), 2.29–2.11 (m, 6H), 1.96 (s, 2H), 1.39 (t, 2H), 0.93 (s, 6H).

4.2.6. 2-((1*H*-pyrrolo[2,3-*b*]pyridin-5-yl)oxy)-4-(4-((4'-chloro-5,5-dimethyl-3,4,5,6-tetrahydro-[1,1'-biphenyl]-2-yl)methyl)piperazin-1-yl)-*N*-((5-(dimethylamino)naphthalen-1-yl)sulfonyl)benzamide (BPFPI)

To the solution of compound 6 (0.86 g, 1.5 mmol) in DMF (30 mL) at 0 °C, isobutyl chloroformate (0.21 mL, 1.65 mmol) as well as *N*-methylmorpholine (0.20 mL, 1.65 mmol) were added and stirred the mixture for 30 min. Dissolve 5-(dimethylamino)naphthalene-1-sulfonamide (0.41g, 1.65 mmol) as well as NaH (0.09g, 1.5 mmol) with DMF (30 mL) and stirred the mixture for 30 min at 80 °C. Mix the two reaction solutions and stirred the mixture for another 8 h at 80 °C. Cool the reaction mixture to room temperature and pour the reaction mixture into the water (120 mL). Extract three times with ethyl acetate and the solvent was removed to give the crude product, followed by purification using silica gel column chromatography. White solid, 0.72 g, yield: 60%, m.p 175–176 °C. ¹H NMR (400 MHz, CDCl₃) δ 10.40 (s, 1H), 9.06 (s, 1H), 8.61 (d, *J* = 7.3 Hz, 1H), 8.57 (d, *J* = 8.6 Hz, 1H), 8.21 (s, 1H), 8.13 (d, *J* = 8.6 Hz, 1H), 7.85 (d, *J* = 8.8 Hz, 1H), 7.70 (s, 1H), 7.61 (t, *J* = 8.0 Hz, 1H), 7.49 (s, 1H), 7.22 (d, *J* = 7.6 Hz, 2H), 7.07 (d, *J* = 7.5 Hz, 1H), 6.90 (d, *J* = 7.3 Hz, 2H), 6.59 (s, 1H), 6.48 (d, *J* = 9.0 Hz, 1H), 5.96 (s, 1H), 3.02 (s, 4H), 2.86 (s, 6H), 2.72 (s, 2H), 2.24–2.08 (m, 6H), 1.95 (s, 2H), 1.40 (t, *J* = 6.0 Hz, 2H), 0.92 (s, 6H). ¹³C NMR (101 MHz, CDCl₃) δ 160.68, 158.29, 154.53, 151.08, 145.33, 144.37, 141.05, 135.68, 134.21, 132.77, 131.41, 130.89, 130.42, 128.74, 128.65, 128.51, 128.02, 127.30, 127.19, 126.30, 122.34, 119.99, 119.76, 117.17, 113.85, 108.19, 108.02, 100.46, 99.67, 59.27, 51.17, 45.89, 44.37, 34.28, 28.68, 28.16, 27.13, 24.54. HRMS (AP-ESI) *m/z*, Calcd for C₄₅H₄₇ClN₆O₄S, ([M+H]⁺): 803.3141, found: 803.3122. HPLC *t*_R = 11.20 min (96.7% purity).

4.2.7. 2-((1*H*-pyrrolo[2,3-*b*]pyridin-5-yl)oxy)-4-(4-((4'-chloro-5,5-dimethyl-3,4,5,6-tetrahydro-[1,1'-biphenyl]-2-yl)methyl)piperazin-1-yl)-*N*-((10-ethyl-9-oxo-9,10-dihydroacridin-2-yl)sulfonyl)benzamide (BPFPI2)

The title compound was synthesized from compound 6 and 10-ethyl-9-oxo-8a,9,10,10a-tetrahydroacridine-2-sulfonamide in a manner similar to that described for the preparation of BPFPI. White solid 0.52 g, yield: 62%. m.p 222–224 °C. ¹H NMR (400 MHz, CDCl₃) δ 10.24 (s, 1H), 9.20 (s, 1H), 9.17 (s, 1H), 8.56 (d, *J* = 8.5 Hz, 2H), 8.26 (s, 1H), 7.93 (d, *J* = 9.0 Hz, 1H), 7.80 (d, *J* = 7.9 Hz, 1H), 7.76

(s, 1H), 7.62 (d, *J* = 8.8 Hz, 1H), 7.57 (d, *J* = 8.6 Hz, 1H), 7.45 (s, 1H), 7.37 (t, *J* = 7.5 Hz, 1H), 7.22 (d, *J* = 7.4 Hz, 2H), 6.90 (d, *J* = 7.6 Hz, 2H), 6.57 (s, 1H), 6.50 (d, *J* = 9.0 Hz, 1H), 5.97 (s, 1H), 4.49 (d, *J* = 7.0 Hz, 2H), 3.49 (s, 2H), 3.04 (s, 4H), 2.73 (s, 2H), 2.28–2.11 (m, 6H), 1.95 (s, 2H), 1.40 (t, *J* = 6.5 Hz, 3H), 0.93 (s, 6H). ¹³C NMR (101 MHz, DMSO) δ 176.56, 173.29, 164.44, 158.44, 154.97, 146.98, 145.92, 143.99, 142.45, 141.63, 135.88, 135.38, 134.84, 132.59, 132.45, 131.30, 130.46, 129.30, 129.19, 128.53, 128.27, 128.12, 127.32, 122.90, 122.52, 120.91, 120.26, 118.54, 117.02, 116.71, 109.16, 102.75, 100.44, 60.11, 52.48, 47.04, 46.77, 41.54, 35.27, 29.32, 28.37, 25.60, 12.76. HRMS (AP-ESI) *m/z*, Calcd for C₄₈H₄₇ClN₆O₅S, ([M+H]⁺): 855.3090, found: 855.3065. HPLC *t*_R = 8.44 min (95.5% purity).

4.2.8. 2-((1*H*-pyrrolo[2,3-*b*]pyridin-5-yl)oxy)-4-(4-((4'-chloro-5,5-dimethyl-3,4,5,6-tetrahydro-[1,1'-biphenyl]-2-yl)methyl)piperazin-1-yl)-*N*-(quinolin-8-yl)benzamide (BPFPI3)

Dissolve compound 6 (0.57 g, 1 mmol) with DMF (30 mL), and DIPEA (0.19 mL, 1.1 mmol) as well as HATU (0.46 g, 1.2 mmol) were added. After 30 min, 8-aminoquinoline (0.15 g, 1.1 mmol) was added and the mixture was stirred for 6 h at 60 °C. Pour the reaction mixture into water (90 mL) and extract three times with ethyl acetate (60 mL × 3). Combine the organic phase and dry it over with MgSO₄. Remove the solvent and the crude product was purified by silica gel chromatography to give white solid 0.49 g, yield: 61%. m.p 114–116 °C. ¹H NMR (400 MHz, CDCl₃) δ 12.24 (s, 1H), 9.40 (s, 1H), 8.99 (d, *J* = 7.7 Hz, 1H), 8.47 (s, 2H), 8.28 (d, *J* = 8.9 Hz, 1H), 8.07 (d, *J* = 8.1 Hz, 1H), 7.80 (s, 1H), 7.55 (t, *J* = 7.9 Hz, 1H), 7.44 (d, *J* = 8.2 Hz, 1H), 7.40 (s, 1H), 7.30 (dd, *J* = 8.1, 4.2 Hz, 1H), 7.24 (s, 1H), 6.94 (d, *J* = 7.6 Hz, 2H), 6.73 (d, *J* = 9.0 Hz, 1H), 6.52 (s, 1H), 6.33 (s, 1H), 3.14 (s, 4H), 2.80 (s, 3H), 2.29 (s, 4H), 2.20 (s, 2H), 1.98 (s, 2H), 1.43 (t, *J* = 6.1 Hz, 2H), 0.95 (s, 6H). ¹³C NMR (101 MHz, CDCl₃) δ 163.35, 157.78, 154.68, 152.61, 148.00, 147.10, 145.66, 142.15, 139.12, 137.05, 135.99, 135.94, 133.58, 131.97, 121.33, 120.99, 120.41, 119.53, 116.88, 114.25, 109.59, 102.46, 101.40, 100.00, 60.41, 52.48, 47.48, 47.03, 38.63, 35.37, 29.23, 28.20, 25.64. HRMS (AP-ESI) *m/z*, Calcd for C₄₂H₄₁ClN₆O₂, ([M+H]⁺): 697.3052, found: 697.3033. HPLC *t*_R = 5.17 min (98.5% purity).

4.2.9. 2-((1*H*-pyrrolo[2,3-*b*]pyridin-5-yl)oxy)-4-(4-((4'-chloro-5,5-dimethyl-3,4,5,6-tetrahydro-[1,1'-biphenyl]-2-yl)methyl)piperazin-1-yl)-*N*-(4-methyl-2-oxo-2*H*-chromen-7-yl)benzamide (BPFPI4)

The title compound was synthesized from compound 6 and 7-amino-4-methylcoumarin in a manner similar to that described for the preparation of BPFPI3. White solid 0.51 g, yield: 47%. m.p 136–138 °C. ¹H NMR (400 MHz, CDCl₃) δ 9.34 (s, 1H), 8.71 (d, *J* = 4.2 Hz, 1H), 8.41 (d, *J* = 8.4 Hz, 1H), 8.21 (d, *J* = 8.4 Hz, 2H), 7.66 (s, 1H), 7.40 (dd, *J* = 10.9, 8.2 Hz, 2H), 7.24 (t, *J* = 7.4 Hz, 2H), 6.93 (d, *J* = 7.3 Hz, 2H), 6.61 (d, *J* = 9.0 Hz, 1H), 6.49 (s, 1H), 6.16 (s, 1H), 3.19 (s, 4H), 2.78 (s, 2H), 2.26–2.24 (m, 5H), 2.19–2.16 (m, 2H), 1.98 (s, 2H), 1.62 (s, 2H), 1.43 (t, *J* = 5.8 Hz, 2H), 0.95 (s, 6H). ¹³C NMR (101 MHz, CDCl₃) δ 162.70, 160.13, 156.57, 151.54, 146.73, 145.80, 142.10, 141.18, 136.75, 135.36, 135.12, 134.59, 131.96, 129.71, 129.35, 129.08, 128.28, 126.53, 120.56, 120.14, 107.89, 102.61, 101.63, 101.29, 60.32, 52.24, 47.01, 46.74, 35.36, 29.23, 28.19, 25.62. HRMS (AP-ESI) *m/z*, Calcd for C₄₃H₄₂ClN₅O₄, ([M+H]⁺): 728.2998, found: 728.2974. HPLC *t*_R = 10.85 min (97.3% purity).

4.3. Fluorescence polarization assay

Recombinant human His-Mcl-1 (250 nM) or His-Bcl-2 (500 nM) was incubated with a range of dilution of the tested BPFPIs for 30 min, followed by the addition of 10 nM 5-FAM Bid-BH3. After incubating for another 20 min, fluorescence polarization was determined using an Envision station (PerkinElmer). The calculations of *K*_i values refer to the previous report [46].

4.4. Fluorescence-spectroscopy test

(a) Absorption spectra of **BPFP1** and **BPFP2** were performed on UV spectrophotometer; (b) The stock solutions of **BPFP1** and **BPFP2** were diluted with PBS buffer (pH 7.4) to the indicated concentrations (5 μ M, 10 μ M, 40 μ M). The fluorescence excitation spectrums and fluorescence emission spectrums were determined on the Thermo-Fisher Varioskan microplate reader; (c) 10 mM stock solutions of **BPFP1** and **BPFP2** were diluted with different solvents (dimethyl sulfoxide, dichloromethane, methanol, acetonitrile, and PBS buffer) to 1 μ M and then fluorescence excitation spectrums as well as fluorescence emission spectrums were determined on the Thermo-Fisher Varioskan microplate reader.

4.5. Fluorescence quantum yield

BPFP1 and **BPFP2** were diluted to the indicated concentration with PBS buffer, and the absorbance of the tested **BPFPs** at excitation wavelength was determined by F-2500 fluorescent spectrophotometer. Fluorescence quantum yields were calculated using the following equation with fluorescein in 0.1 M NaOH ($\Phi_{ST} = 0.92$) as the reference.

$$\Phi_X = \Phi_{ST} (A_{ST}/A_X)(F_X/F_{ST})(\eta_X/\eta_{ST})$$

Where Φ is the fluorescence quantum yield; the subscript ST denotes the reference and subscript X denotes the sample; F is the integrated area under the fluorescence spectra at the excitation wavelength; A is the absorbance at the excitation wavelength; and η is the refractive index of the solvent.

4.6. Fluorescent properties of **BPFPs** incubated with Bcl-2 or Mcl-1 protein

Serial concentrations (0.0125 mg/mL, 0.025 mg/mL, 0.05 mg/mL, 0.075 mg/mL, 0.10 mg/mL mg/mL and 0.125 mg/mL) of Bcl-2 protein or Mcl-1 protein were incubated with 2 μ M **BPFP1** for 20 min and then fluorescence emission spectra were determined on the Thermo-Fisher Varioskan microplate reader. Besides, the fluorescence emission spectra of 2 μ M **BPFP1** treated with 0.125 mg/mL Bcl-2 protein in the presence or absence of ABT-199 (10 μ M) was also determined in a similar manner.

4.7. Cell culture and cytotoxicity studies

ACHN cells and HL-60 cells were cultured in RPMI1640 medium containing 10% FBS. HUVECs were cultured with RPMI1640 medium containing 10% FBS and 0.1% heparin.

For cytotoxicity studies, ACHN cells, HL-60 cells, and HUVECs were seeded in a 96-well plate and incubated for 8 h. Following treatment with the indicated dilution of **BPFP1** and ABT-199 for 1 h, CCK-8 solution was added. After incubating the mixture at 37 $^{\circ}$ C for another 4 h, absorbance was measured with a microtiter-plate reader at 570 nm.

4.8. Fluorescence imaging and colocalization analysis

Carcinoma cells (ACHN cells) and normal-tissue cells (HUVECs) were selected for fluorescence imaging. ACHN cells and HUVECs (1×10^5) were seeded into small bowl, and incubated for 8h. Upon treatment with 1 μ M **BPFP1** for 20 min, fluorescence was monitored using a Zeiss Axio Observer A1 fluorescence microscope (objective lens: 63 \times). Competitive imaging assays were conducted by co-incubating **BPFP1** (1 μ M), ABT-199 (5 μ M) and cells.

For fluorescence colocalization analysis, cells were co-incubated

with **BPFP1** (1 μ M), mitochondrial dye (300 nM MitoTracker Red CMXRos) and nuclear dye (10 μ g/mL Hoechst 33342) for 20 min. Fluorescence imaging was conducted using a Zeiss LSM780 confocal fluorescence microscope.

4.9. Flow-cytometry analysis

Cells (1×10^5 cells/well) were cultured for 8 h in a 6-well plate, and then incubated with **BPFP1** (1 μ M) in the presence or absence of ABT-199 (5 μ M) for 20 min. The cells were then harvested and analyzed using a Beckman Coulter MoFloAstrios EQ Flow Cytometer.

4.10. Cell sorting

A solid tumor model and a hematoma model were constructed to simulate the composition of tumor tissue using carcinoma cells (ACHN and HL-60 cells) and normal-tissue cells (HUVECs). Briefly, the solid tumor model contains ACHN cells and HUVECs, and the hematoma model consisted of HL-60 cells and HUVECs. The two models were incubated with 1 μ M **BPFP1** for 20 min, followed by analysis with a Beckman Coulter MoFloAstrios EQ Flow Cytometer.

4.11. Cell line identification

Short tandem repeat (STR) analysis was applied for cell line identification. Cells obtained from cell sorting were collected by centrifugation (800 rpm, 10 min) and cell precipitation were lysed. Cellular DNA was extracted and purified with a Lifefeng DNA kit. PCR is amplified with a human STR amplification fluorescence detection kit and STR profiles of the cell line samples were assayed with a 3730xl DNA Analyzer (Applied Biosystems). The STR profiles of the samples were searched and analyzed in two recognized repositories (ATCC, DSMZ) to identify the cell lines.

4.12. Western blot

Treated or untreated cells (ACHN cells, HL-60 cells, and HUVECs) were lysed with 1 \times RIPA buffer containing 1 mM PMSF on ice for 30 min. The supernatant was collected by centrifugation (4 $^{\circ}$ C, 14000 rpm, 10 min), and then boiled in loading buffer. Samples were electrophoretically separated on 12.5% SDS PAGE gel and transferred to PVDF membrane. After being blocked with 5% nonfat dry milk and washed with TBST, the membranes were co-incubated with primary antibodies of Bcl-2 protein (Cell Signaling Technology, Cat. 4223) overnight at 4 $^{\circ}$ C. The PVDF membrane was washed with TBST and then incubated with secondary antibody, followed by ECL reaction. Images of the member were then captured with an Amersham Imager 680.

4.13. Docking studies

The solution structure of the anti-apoptotic protein Bcl-2 (PDB ID: 2O2F) was chosen for docking studies by means of GLIDE (version 11.5, Schrodinger). After protein preparation and grid generation, ABT-199, **BPFP1** or **BPFP2** was docked into the binding site of Bcl-2 protein. Then, top-scoring binding poses were selected as the proposed binding modes.

Declaration of competing interest

The authors declare that they have no known competing financial interests or personal relationships that could have appeared to influence the work reported in this paper.

Acknowledgement

We genuinely thank the Advanced Medical Research Institute, Shandong University, for their help in the experiments. We thank Renxiao Wang from Fudan University for his help in the biological evaluations. This work was supported by the National Nature Science Foundation of China (21672127 and 81874288), the Shandong Provincial Natural Science Foundation (ZR2019LZL004) and the Fundamental Research Funds of Shandong University (Grant No. 2018JC017).

Abbreviations

BFPF	Bcl-2 protein fluorescence probe
ABT-199	Venetoclax, a highly potent and selective Bcl-2 inhibitor
HATU	1-[bis(dimethylamino)methylene]-1H-1,2,3-triazolo [4,5-b]pyridinium 3-oxid hexafluorophosphate
DIPEA	<i>N,N</i> -diisopropylethylamine;
DMF	<i>N,N</i> -dimethylformamide;
Ki	inhibition constant
PBS buffer	phosphate buffer saline;
ACHN	human renal carcinoma cells
HL-60	human acute promyelocytic leukemia cells
HUVEC	human umbilical vein endothelial cells
CKK-8	cell counting kit
RIPA	RIPA lysis buffer
PMSF	phenylmethanesulfonyl fluoride, protease inhibitors
SDS	sodium dodecylsulfate
PAGE	polyacrylamide gel electrophoresis
PVDF	polyvinylidene fluoride;
GAPDH	glyceraldehyde-3-phosphate dehydrogenase
TBST	tris buffered saline tween
ECL	electrochemiluminescence
GAPDH	glyceraldehyde-3-phosphate dehydrogenase
STR	short tandem repeat
ATCC	American type culture collection
DSMZ	Deutsche Sammlung von Mikroorganismen und Zellkulturen GmbH
FCM	flow-cytometry
DMSO	dimethyl sulfoxide

Appendix A. Supplementary data

Supplementary data to this article can be found online at <https://doi.org/10.1016/j.ejmech.2021.113725>.

References

- [1] R.L. Siegel, K.D. Miller, J.A. Emal, Cancer statistics, *Ca - Cancer J. Clin.* 70 (2020) 7–30.
- [2] C.E. DeSantis, K.D. Miller, A. Goding Sauer, A. J. Emal, R.L. Siegel, Cancer statistics for African Americans, *Ca - Cancer J. Clin.* 69 (2019) 211–233.
- [3] F. Bray, J. Ferlay, I. Soerjomataram, R.L. Siegel, L.A. Torre, A. Jemal, Global cancer statistics 2018: GLOBOCAN estimates of incidence and mortality worldwide for 36 cancers in 185 countries, *Ca - Cancer J. Clin.* 68 (2018) 394–424.
- [4] R.L. Siegel, K.D. Miller, A. Jemal, Cancer statistics, *Ca - Cancer J. Clin.* 67 (2017) 7–30.
- [5] R.L. Siegel, K.D. Miller, A. Jemal, Cancer statistics, *Ca - Cancer J. Clin.* 66 (2016) 2016) 7–30.
- [6] A. Jemal, F. Bray, M.M. Center, J. Ferlay, E. Ward, D. Forman, Global cancer statistics, *Ca - Cancer J. Clin.* 61 (2011) 69–90.
- [7] K.D. Miller, R.L. Siegel, C.C. Lin, A.B. Mariotto, J.L. Kramer, J.H. Rowland, K.D. Stein, R. Alteri, A. Jemal, Cancer treatment and survivorship statistics, *Ca - Cancer J. Clin.* 66 (2016) 271–289.
- [8] R. Siegel, C. DeSantis, K. Virgo, K. Stein, A. Mariotto, T. Smith, D. Cooper, T. Gansler, C. Lerro, S. Fedewa, C. Lin, C. Leach, R.S. Cannady, H. Cho, S. Scoppa, M. Hachey, R. Kirch, A. Jemal, E. Ward, Cancer treatment and survivorship statistics, *Ca - Cancer J. Clin.* 62 (2012) 220–241.
- [9] L.A. Torre, B. Trabert, C.E. DeSantis, K.D. Miller, G. Samimi, C.D. Runowicz, M.M. Gaudet, A. Jemal, R.L. Siegel, Ovarian cancer statistics, *Ca - Cancer J. Clin.* 68 (2018) 284–296.
- [10] N. Hawkes, Cancer survival data emphasise importance of early diagnosis, *BMJ* 364 (2019) 1408.
- [11] M.A. Richards, The national Awareness and early diagnosis initiative in England: assembling the evidence, *Br. J. Canc.* 101 (2009) S1–S4.
- [12] C.S. Thomson, D. Forman, Cancer survival in England and the influence of early diagnosis: what can we learn from recent EUROcare results? *Br. J. Canc.* 101 (2009) S102–S109.
- [13] N. Houssami, S. Ciatto, F. Martinelli, R. Bonardi, S.W. Duffy, Early detection of second breast cancers improves prognosis in breast cancer survivors, *Ann. Oncol.* 20 (2009) 1505–1510.
- [14] S. Sugumaran, M.F. Jamlos, M.N. Ahmad, C.S. Bellan, D. Schreurs, Nanostructured materials with plasmonic nanobiosensors for early cancer detection: a past and future prospect, *Biosens. Bioelectron.* 100 (2018) 361–373.
- [15] S.H. Jafari, Z. Saadatpour, A. Salmaninejad, F. Momeni, M. Mokhtari, J.S. Nahand, M. Rahmati, H. Mirzaei, M. Kianmehr, Breast cancer diagnosis: imaging techniques and biochemical markers, *J. Cell. Physiol.* 233 (2018) 5200–5213.
- [16] E. Siminska, M. Koba, Amino acid profiling as a method of discovering biomarkers for early diagnosis of cancer, *Amino Acids* 48 (2016) 1339–1345.
- [17] C. Uhler, G.V. Shivashankar, Nuclear mechanopathology and cancer diagnosis, *Trends Cancer* 4 (2018) 320–331.
- [18] H. Li, G. Hong, H. Xu, Z. Guo, Application of the rank-based method to DNA methylation for cancer diagnosis, *Gene* 555 (2015) 203–207.
- [19] F.J. Nassar, R. Nasr, R. Talhouk, MicroRNAs as biomarkers for early breast cancer diagnosis, prognosis and therapy prediction, *Pharmacol. Ther.* 172 (2017) 34–49.
- [20] D. Weller, P. Vedsted, G. Rubin, F.M. Walter, J. Emery, S. Scott, C. Campbell, R.S. Andersen, W. Hamilton, F. Olesen, P. Rose, S. Nafees, E. van Rijswijk, S. Hiom, C. Muth, M. Beyer, R.D. Neal, The Aarhus statement: improving design and reporting of studies on early cancer diagnosis, *Br. J. Canc.* 106 (2012) 1262–1267.
- [21] J.E. Chipuk, T. Moldoveanu, F. Llambi, M.J. Parsons, D.R. Green, The BCL-2 family reunion, *Mol. Cell.* 37 (2010) 299–310.
- [22] J.C. Martinou, R.J. Youle, Mitochondria in apoptosis: Bcl-2 family members and mitochondrial dynamics, *Dev. Cell* 21 (2011) 92–101.
- [23] R.J. Youle, A. Strasser, The BCL-2 protein family: opposing activities that mediate cell death, *Nat. Rev. Mol. Cell Biol.* 9 (2008) 47–59.
- [24] J.M.C. Adams, The Bcl-2 protein family, Arbiters of cell survival, *Science* 281 (1998) 1322–1326.
- [25] M. Kvanakul, M.G. Hinds, The Bcl-2 family: structures, interactions and targets for drug discovery, *Apoptosis* 20 (2015) 136–150.
- [26] P.E. Czabotar, G. Lessene, A. Strasser, J.M. Adams, Control of apoptosis by the BCL-2 protein family: implications for physiology and therapy, *Nat. Rev. Mol. Cell Biol.* 15 (2014) 49–63.
- [27] D.N.G. Hockenbery, C. Millman, R.D. Schreiber, S.J. Korsmeyer, Bcl-2 is an inner mitochondrial membrane protein that blocks programmed cell death, *Nature* 348 (1990) 334–336.
- [28] P.N. Kelly, A. Strasser, The role of Bcl-2 and its pro-survival relatives in tumorigenesis and cancer therapy, *Cell Death Differ.* 18 (2011) 1414–1424.
- [29] T. Oltersdorf, S.W. Elmore, A.R. Shoemaker, et al., An inhibitor of Bcl-2 family proteins induces regression of solid tumours, *Nature* 435 (2005) 677–681.
- [30] S. Krajewski, M. Krajewska, J. Ehrmann, M. Sikorska, B. Lach, J. Chatten, J.C. Reed, Immunohistochemical analysis of Bcl-2, Bcl-X, Mcl-1, and Bax in tumors of central and peripheral nervous system origin, *Am. J. Pathol.* 150 (1997) 805–814.
- [31] A. Huang, P.D. Fone, R. Gandour-Edwards, R.W.D. White, R.K. Low, Immunohistochemical analysis of BCL-2 protein expression in renal cell carcinoma, *J. Urol.* 162 (1999) 610–613.
- [32] B. Kiss, V. Skuginna, A. Fleischmann, R.H. Bell, C. Collins, G.N. Thalmann, R. Seiler, Bcl-2 predicts response to neoadjuvant chemotherapy and is overexpressed in lymph node metastases of urothelial cancer of the bladder, *Urol. Oncol.* 33 (2015) 166, e1–e8.
- [33] D.M.Q.F.G. Harnois, A. Celli, N.F. LaRusso, G.J. Gores, Bcl-2 is overexpressed and alters the threshold for apoptosis in a cholangiocarcinoma cell line, *Hepatology* 4 (1997) 884–890.
- [34] F. Vaillant, D. Merino, L. Lee, K. Breslin, B. Pal, M.E. Ritchie, G.K. Smyth, M. Christie, L.J. Phillipson, C.J. Burns, G.B. Mann, J.E. Visvader, G.J. Lindeman, Targeting BCL-2 with the BH3 mimetic ABT-199 in estrogen receptor-positive breast cancer, *Canc. Cell* 24 (2013) 120–129.
- [35] J. Qi, C. Chen, X. Zhang, X. Hu, S. Ji, R.T.K. Kwok, J.W.Y. Lam, D. Ding, B.Z. Tang, Light-driven transformable optical agent with adaptive functions for boosting cancer surgery outcomes, *Nat. Commun.* 9 (2018) 1848.
- [36] X. Liu, L. Wang, X. Xu, H. Zhao, W. Jiang, Endogenous stimuli-responsive nucleus-targeted nanocarrier for intracellular mRNA imaging and drug delivery, *ACS Appl. Mater. Interfaces* 10 (2018) 39524–39531.
- [37] Y. Takaoka, A. Ojida, I. Hamachi, Protein organic chemistry and applications for labeling and engineering in live-cell systems, *Angew. Chem. Int. Ed. Engl.* 52 (2013) 4088–4106.
- [38] Y. Liu, X. Zhang, Y.L. Tan, G. Bhabha, D.C. Ekiert, Y. Kipnis, S. Bjelic, D. Baker, J.W. Kelly, De novo-designed enzymes as small-molecule-regulated fluorescence imaging tags and fluorescent reporters, *J. Am. Chem. Soc.* 136 (2014) 13102–13105.
- [39] T. Liu, G. Dong, F. Xu, B. Han, H. Fang, Y. Huang, Y. Zhou, L. Du, M. Li, Discovery

- of turn-on fluorescent probes for detecting Bcl-2 protein, *Anal. Chem.* 91 (2019) 5722–5728.
- [40] L. Wang, D.T. Sloper, S.N. Addo, D. Tian, W.J. Slaton, C. Xing, WL-276, an antagonist against Bcl-2 proteins, overcomes drug resistance and suppresses prostate tumor growth, *Cancer Res* 68 (2008) 4377–4383.
- [41] S.M. O'Brien, D.F. Claxton, M. Crump, S. Faderl, T. Kipps, M.J. Keating, J. Viallet, B.D. Cheson, Phase I study of obatoclax mesylate (GX15-070), a small molecule pan-Bcl-2 family antagonist, in patients with advanced chronic lymphocytic leukemia, *Blood* 113 (2009) 299–305.
- [42] M.F. van Delft, A.H. Wei, K.D. Mason, C.J. Vandenberg, L. Chen, et al., The BH3 mimetic ABT-737 targets selective Bcl-2 proteins and efficiently induces apoptosis via Bak/Bax if Mcl-1 is neutralized, *Canc. Cell* 10 (2006) 389–399.
- [43] C. Tse, A.R. Shoemaker, J. Adickes, M.G. Anderson, J. Chen, S. Jin, et al., ABT-263: a potent and orally bioavailable Bcl-2 family inhibitor, *Cancer Res* 68 (2008) 3421–3428.
- [44] M.S. Davids, A. Letai, ABT-199: taking dead aim at BCL-2, *Canc. Cell* 23 (2013) 139–141.
- [45] J. Yang, X. Liu, K. Bhalla, C.N. Kim, A.M. Ibrado, J. Cai, T.I. Peng, D.P. Jones, X. Wang, Prevention of apoptosis by Bcl-2, release of cytochrome c from mitochondria blocked, *Science* 275 (1997) 1129–1132.
- [46] Z. Nikolovska-Coleska, R. Wang, X. Fang, H. Pan, Y. Tomita, P. Li, P.P. Roller, K. Krajewski, N.G. Saito, J.A. Stuckey, S. Wang, Development and optimization of a binding assay for the XIAP BIR3 domain using fluorescence polarization, *Anal. Biochem.* 332 (2004) 261–273.